Shielding of the azimuthal magnetic field by the anode plasma in a relativistic self-magnetic-pinch diode

S. Biswas,[1] M. D. Johnston,[2] R. Doron,[1] D. Mikitchuk,[1] Y. Maron,[1] S. G. Patel,[2] M. L. Kiefer,[2] and M. E. Cuneo[2]
[1]*Weizmann Institute of Science, Rehovot 7610001, Israel*
[2]*Sandia National Laboratories, Albuquerque, New Mexico 87185, USA*

(Received 3 July 2018; accepted 16 October 2018; published online 26 November 2018)

In relativistic electron beam diodes, the self-generated magnetic field causes electron-beam focusing at the center of the anode. Generally, plasma is formed all over the anode surface during and after the process of the beam focusing. In this work, we use visible-light Zeeman-effect spectroscopy for the determination of the magnetic field in the anode plasma in the Sandia 10 MV, 200 kA (RITS-6) electron beam diode. The magnetic field is determined from the Zeeman-dominated shapes of the Al III 4*s*–4*p* and C IV 3*s*–3*p* doublet emissions from various radial positions. Near the anode surface, due to the high plasma density, the spectral line-shapes are Stark-dominated, and only an upper limit of the magnetic field can be determined. The line-shape analysis also yields the plasma density. The data yield quantitatively the magnetic-field shielding in the plasma. The magnetic-field distribution in the plasma is compared to the field-diffusion prediction and found to be consistent with the Spitzer resistivity, estimated using the electron temperature and charge-state distribution determined from line intensity ratios. *Published by AIP Publishing.*
https://doi.org/10.1063/1.5046945

I. INTRODUCTION

The Self-Magnetic-Pinch (SMP) diode is being investigated for use as a high-brightness, flash x-ray radiographic source.[1–4] The SMP diode is capable of producing >350 Rads at 1 m with a 1.7 mm FWHM x-ray spot size during a 50 ns pulse duration. The diode operates at an endpoint energy of ~7.5 MeV and draws a total current of ~120 kA. The diode consists of a small, hollowed, cylindrical metal cathode and a solid, flat-plate anode. An electron beam is generated at the tip of the cathode by explosive emission and accelerates across an ~1 cm vacuum A–K gap onto the anode surface, where it interacts with a high atomic number material (tantalum or tungsten), producing bremsstrahlung x-rays and forming a dense surface plasma.[5] As the electron beam rapidly heats the surface of the anode, space-charged ion emission from the anode surface charge neutralizes the electron beam, resulting in increased current and pinching of the electron-beam due to self-magnetic effects.[6] Determination of this magnetic field distribution is essential for the understanding of the pinch dynamics and, in particular, for controlling the size of the x-ray source.

Spectroscopic measurements based on the Zeeman splitting have been previously applied to determine the magnetic field and its penetration into the anode plasma in a magnetically insulated ion-beam diode.[7] In that study, the plasma was found to be penetrated by the fast-rising diamagnetic-field component in the diode; no magnetic-field shielding by the plasma was observed. This fast field penetration corresponded to a resistivity that is <10× of the Spitzer resistivity, which was later explained[8] by the lower-hybrid-drift instability. Recently, we demonstrated the use of the Zeeman effect to determine the azimuthal magnetic field near the anode surface in the SMP diode addressed here.[9]

In the present work, we report on the use of the Zeeman effect to determine the radial distribution of the azimuthal magnetic field in the diode as a function of the distance from the anode surface. This measurement yielded the shielding of the magnetic field by the anode plasma during the focusing of the electron beam. The measurements utilize the line-spectra of Al III and C IV collected from the anode plasma along multiple chords and at two different axial positions across a 1-mm distance from the anode surface. In fact, it is shown that these data provide information on three axial positions, based on the different axial propagations of the Al III and C IV ions.

In addition, since the data are chordally integrated, they required an Abel inversion of the observed line shapes ("onion-peeling" technique[10]) in order to obtain the line shapes from which the radially resolved magnetic field can be expected. For the conditions of the SMP diode, Zeeman splitting cannot always be resolved due to the large Stark broadening in the high-density plasma formed over the anode surface. For these cases, detailed line-shape analysis,[11–13] considering the Stark and Doppler broadenings, the instrumental response, and the Zeeman-effect contribution, is made for obtaining the information on the magnetic field and plasma density. Due to this rather complex line-shape processing, the data from the inner radii mainly allowed for determining an upper limit for the magnetic fields. The spectra from the outer radii, however, yielded the magnetic field amplitude as a function of the distance from the anode surface, demonstrating the shielding of the magnetic field by the anode plasma as a function of the axial distance (<1 mm) from the anode surface. These data allowed for comparisons with solutions of the magnetic-field diffusion equation to be made. The plasma resistivity inferred from these comparisons was found to be comparable to the Spitzer resistivity where the latter was obtained from the electron temperature (T_e) determined from the line-intensity ratios in the plasma and the average ionic charge-state. The line shape modeling that also yielded the electron density radial distribution in the plasma will be discussed in a subsequent report.

To the best of our knowledge, these studies represent the first time measurements of the magnetic field and the determination of the magnetic-field shielding in a particle-beam diode.

II. SCHEMATIC OF THE MEASUREMENTS

The experiment was performed in the SMP diode of the RITS-6 accelerator facility at Sandia National Laboratories.[3] Light emission from the anode plasma was used for obtaining information on the plasma properties and the spatial distribution of the azimuthal magnetic field (B_θ) of the diode. The spectroscopy data were collected with a fast-gated (<7 ns) ICCD camera, using a multi-fiber array, with a lens coupled to a 0.32-m aberration-corrected spectrometer with a spectral resolution of 0.5 Å. Light was collected from the SMP diode using a 50-mm, 150-mm focal length, glass achromat. The fiber array was positioned so that each fiber imaged light from a 0.5-mm focal region close to the anode surface. There was a demagnification of 5× from the imaged plasma light to the collection fiber outside the chamber, resulting in a collection area of 0.5-mm in diameter throughout the plasma volume. The fiber array consisted of 100 μm-diameter silica fibers about 10 m long, transmitting the light to a shielded screen room, where it was reimaged using an f/# matching double achromatic pair onto the slit of the spectrometer.

A schematic description of the measurement is shown in Fig. 1. Two sets of fiber arrays were used for collecting light from different radial and axial positions. As shown in Fig. 1, one set of fibers collected light from a 0.5-mm-diameter region near the anode surface ($0 \le z \le 0.5$ mm) and the second set from the region 0.5 mm $\le z \le 1.0$ mm, where $z = 0$ is the anode surface.

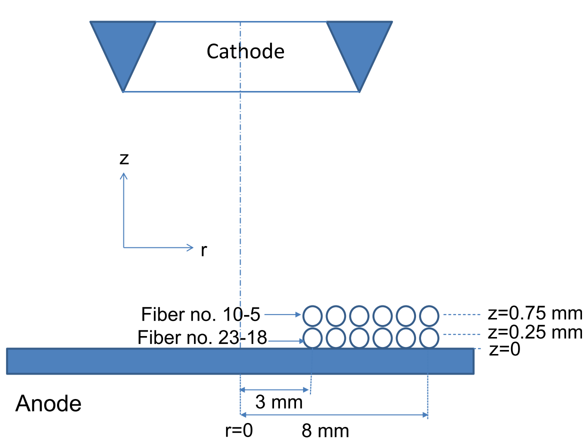

FIG. 1. Schematic of the measurement.

III. MEASUREMENTS

Figure 2 shows the spectra recorded from different radial and axial positions in shot 2028. The left panel presents the spectra recorded from the region at $0 \le z \le 0.5$ mm, and the right panel presents the spectra recorded from the region further away from the anode, at $0.5 \le z \le 1$ mm. The spectra far from the anode surface [Figs. 2(g)–2(l)] clearly show the Al III doublet transition $4s\,^2S_{1/2} - 4p\,^2P_{1/2,3/2}$ (5996 and 5722 Å) and C IV doublet transition $3s\,^2S_{1/2} - 3p\,^2P_{1/2,3/2}$ (5801 and 5812 Å), whereas in the spectra from near the anode surface, only the Al III $4s\,^2S_{1/2} - 4p\,^2P_{1/2,3/2}$ doublet is clearly observed and the C IV $3s\,^2S_{1/2} - 3p\,^2P_{1/2,3/2}$ doublet is very weak.

The radial distribution of the relative intensities of the Al III 5722 Å and C IV 5812 Å emissions is shown in Fig. 3. Presented are both the chordally integrated data and their inverse-Abel transform. For performing the inverse-Abel transform, we assumed that the intensity falls linearly to 0 at $r = 9$ mm. This assumption is based on the results of a similar experiment, not presented here, showing a rapid intensity decrease in the region of $r = 8$–9 mm. The intensities of each transition are normalized by their maximum values. The figure illustrates that near the anode surface, at $0 \le z \le 0.5$ mm, the intensities of both Al III and C IV lines have a peak at $r = 4$ mm. For 0.5 mm $\le z \le 1.0$ mm, the intensity of the Al III line is nearly constant throughout r; the intensity of the C IV line is maximum at the edge ($r = 8$ mm) and falls towards the center. It can also be seen that near the edge of the plasma in the radial direction, the Al III is mainly emitted from a region close to the anode surface (small z-values), whereas the C IV is from larger z. This is probably due to the fact that carbon is absorbed on the aluminum anode surface. Therefore, when the electron beam hits the anode surface, carbon comes out first and becomes ionized forming C IV. In addition, the C IV is expected to expand faster due to its higher charge-to-mass ratio.

IV. DATA ANALYSIS

The spectral line-shapes are used to determine the magnetic field and electron density. Since the experimental spectra are chordally integrated, in order to obtain the line-shape as a function of r, the inverse-Abel transform has been performed. Here, we employ an "onion-peeling" approach,[10] assuming that the plasma boundary is at $r = 8$ mm. The chordal spectrum obtained for each distance y from the anode center is the summation of spectra along that chord. The analysis begins by analyzing the line shape observed at $y = 8$ mm, assuming no plasma emission at $r > 8$ mm. Then, the line shape at $y = 7$ mm is assumed to be the sum of the line shapes from $r = 7$ mm and from $r = 8$ mm, as seen along the chord $y = 7$ mm. Thus, the line shape for $r = 7$ mm is obtained by subtracting from the spectrum at $y = 7$ mm [Figs. 2(e) and 2(k)] the contribution of the line shape for $r = 8$ mm. The intensity and line-shape of this contribution are known from the measurement at $y = 8$ mm, modified according to the change in the angle between B_θ at $r = 8$ mm and the observation direction (for $y = 8$ mm, B_θ is parallel to the line of sight, and for $y = 7$ mm, B_θ of $r = 8$ mm is at an

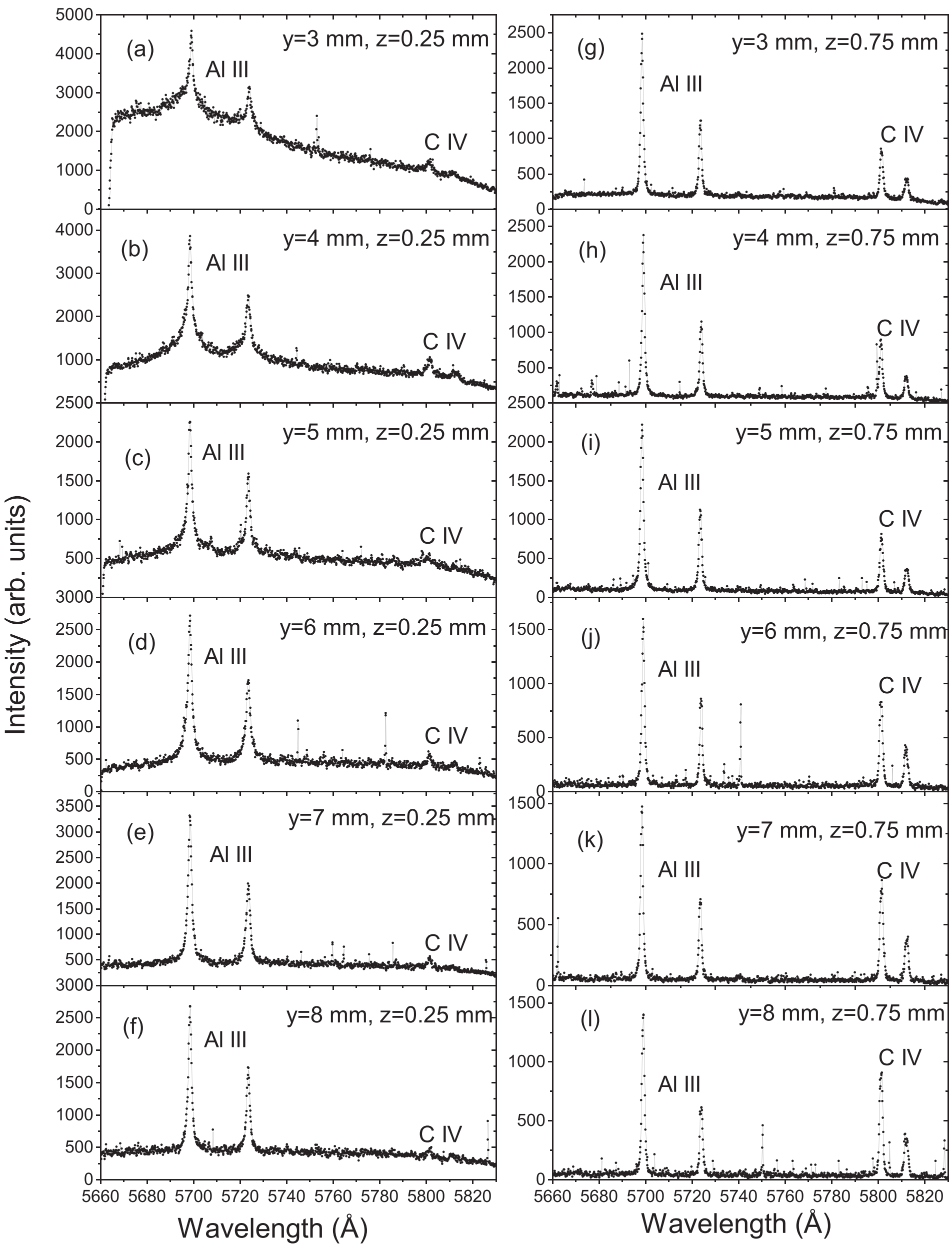

FIG. 2. Recorded chordally integrated spectra at different radial positions using two sets of fiber arrays. The spectra in the left panels, (a)–(f), are from the region adjacent to the anode surface and, in the right panels, (g)–(l), from the region at 0.75 mm away from the anode surface.

angle $\theta > 0°$ relative to the line of sight). The procedure is then repeated for each $y < 7$ mm.

In the "onion peeling" process, we assume that the plasma radial boundary is at $r = 8$ mm since this is the maximum radius for which the signals are large enough to allow for line shape measurements. It is proven rigorously that neglecting the minuscule emission at $r = 9$ mm causes no significant error in this analysis.

To determine B_θ, first calculated are Zeeman profiles for different fields. Subsequently, each Zeeman profile is convolved with a Lorentzian (Stark broadening) and a Gaussian which is the known instrumental resolution of FWHM ~0.5 Å. The simulated spectra are compared with the Abel-inverted spectrum, and the value of B_θ and the Stark width are then varied to obtain the best fit (minimum of χ^2) to the spectrum, using the same procedure as in Refs. 11–13. We note that the Doppler broadening is negligible here. It can be estimated either by assuming $T_i = T_e \approxeq 5$ eV (T_e is measured from the C III and C IV line-intensity ratios in another experiment[9,14]) or from visible imaging,[9] where the ion velocities parallel to the anode surface were found to be ≈1.4 cm/μs.

In the analysis, we only fit the (1/2–1/2) component of the doublet, owing to its higher sensitivity to the magnetic field. The experimental intensity ratio (1/2–3/2)/(1/2–1/2), expected to be 2, is found to be between 2 and 2.2. The deviation from a value of 2 can be either due to errors in the measurement or impurities contributing to the (1/2–3/2) component. For the case of the Al III, a C III impurity at 5695.9 Å can affect the (1/2–3/2) component. Therefore, simulating the (1/2–3/2) shape does not help to further constrain B_θ.

Figure 4 presents the experimental data of the Al III $4s - 4p\,^3S_{1/2} - {}^3P_{1/2}$ component at different radii for 0.5 mm $\leq z \leq 1.0$ mm after the inverse-Abel transform, together with their best fits. Figure 5 gives the same for the C IV $3s - 3p\,^3S_{1/2} - {}^3P_{1/2}$ component. Evidently, the inverse-Abel procedure introduces additional uncertainties in

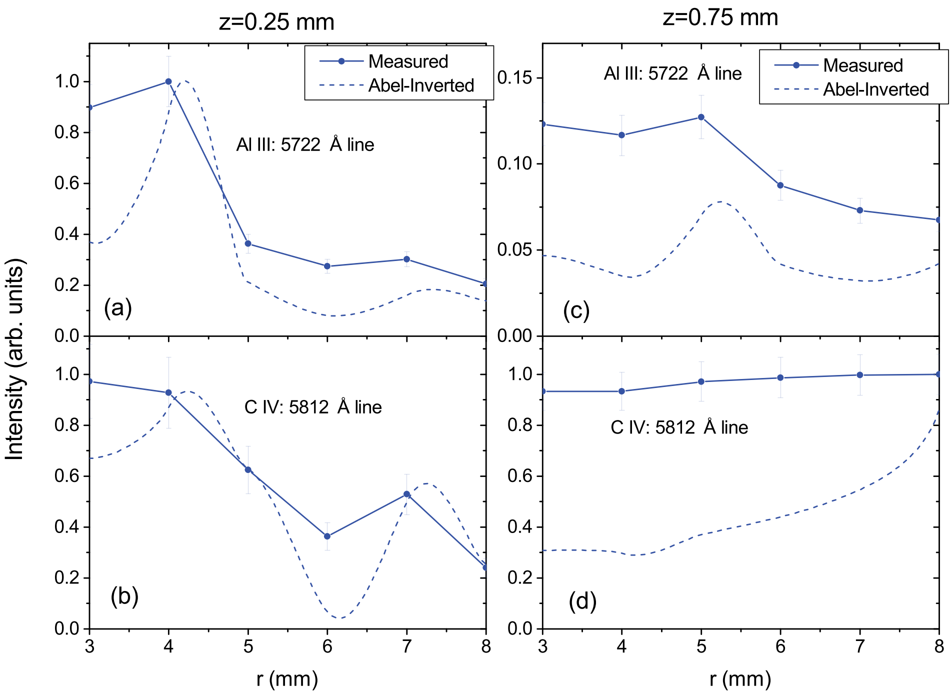

FIG. 3. Radial distribution of the relative line intensities of Al III 5722 Å and C IV 5812 Å. Left and right panels represent the emissions from $z = 0.25$ mm and $z = 0.75$ mm, respectively. The solid lines and the dashed lines represent the measured chordally integrated and Abel-inverted intensities, respectively.

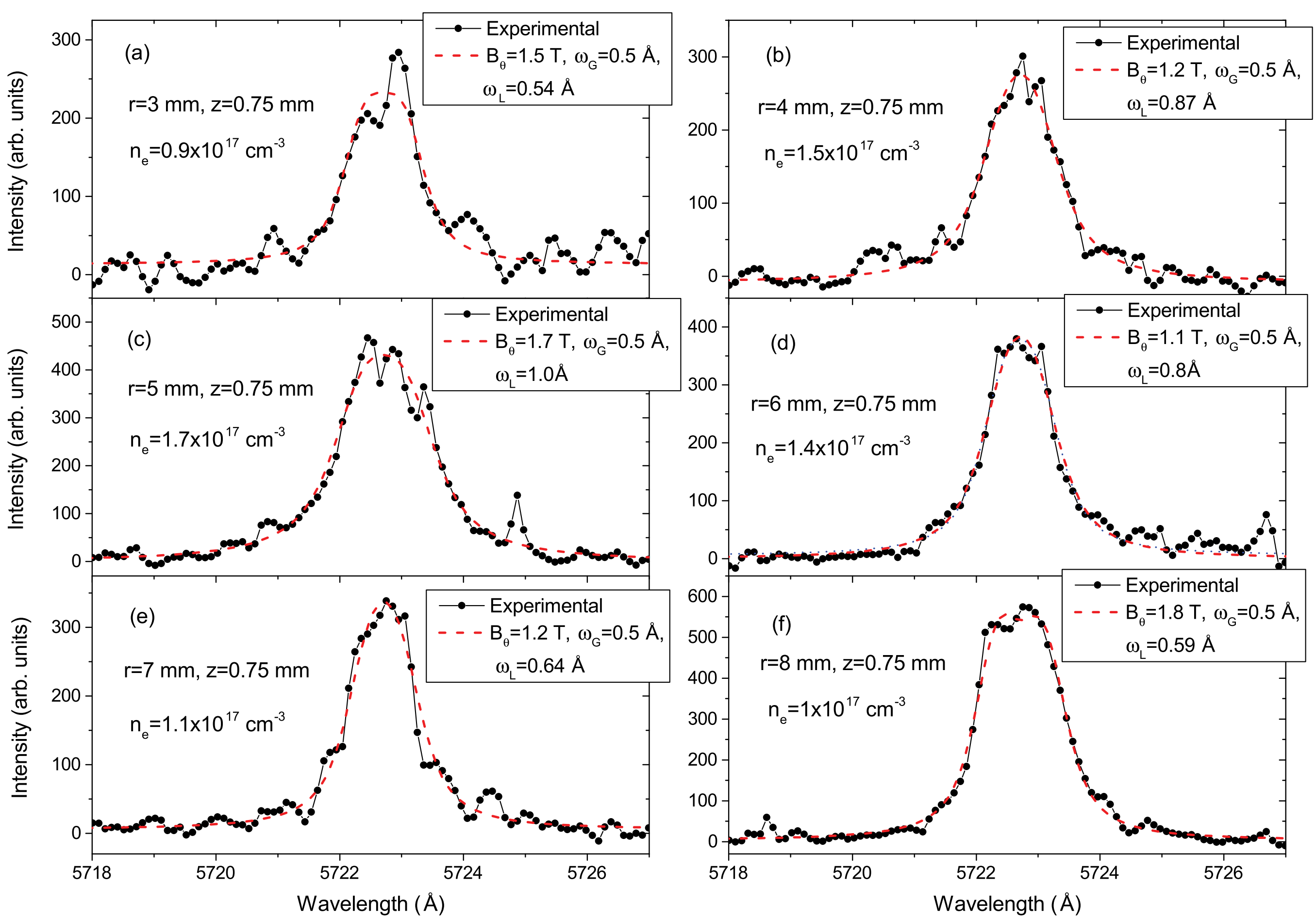

FIG. 4. Al III $4s - 4p\ ^3S_{1/2} - {}^3P_{1/2}$ component from the region $0.5\,\text{mm} \leq z \leq 1.0\,\text{mm}$ at different radii after Inverse-Abel transform. Dashed (red) curves are the simulated spectra obtained by convolving the Zeeman pattern with the Stark-Lorentzian and Instrumental-Gaussian profiles. In the figure, B_θ, ω_L, and ω_G are the azimuthal magnetic field value, Stark FWHM, and instrumental FWHM used for the fit, respectively; n_e is the electron density corresponding to ω_L.

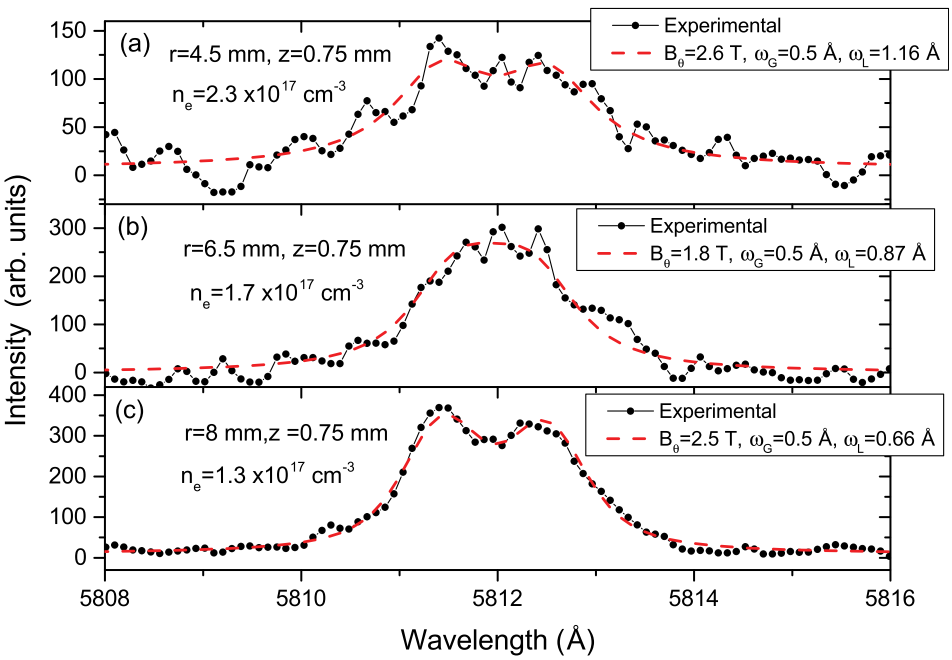

FIG. 5. C IV $3s - 3p\,^3S_{1/2} - ^3P_{1/2}$ component from the region $0.5\,\text{mm} \le z \le 1.0\,\text{mm}$ at different radii after Inverse-Abel transformation. Dashed (red) curves are the simulated spectra obtained by convolving the Zeeman profile with the Stark-Lorentzian and Instrumental-Gaussian profiles. In the figure, B_θ, ω_L, and ω_G are the azimuthal magnetic field value, Stark FWHM, and instrumental FWHM, used for the fit, respectively; n_e is the electron density estimated from ω_L.

the experimental data and reduces the signal-to-noise ratios (SNR) for $r < 8$ mm. This effect is particularly strong for C IV due to the lower intensity for smaller r [see Fig. 3(d)]. Therefore, for C IV, the fitting is performed by averaging the data for $r = 4$ and 5 mm and for $r = 6$ and 7 mm. These are attributed to $r = 4.5$ and 6.5 mm, respectively. The SNR for $r = 3$ mm is too poor to be useful.

The parameters that yielded the best least-square fits are given in Figs. 4 and 5. The electron density (n_e) that corresponds to each Stark-Lorentzian width[12,15,16] is also given in the figure. The values of n_e are between 1×10^{17} and $2 \times 10^{17}\,\text{cm}^{-3}$. An analysis of $n_e(r, z)$ in the diode will be given in a subsequent report. The n_e obtained was also used to estimate the opacity effect. The values of the optical depth (τ) were found to be much less than 1 by considering the ion density $n_i = n_e/Z$, with Z the ionic charge and a plasma extent of 1 cm. This gives an upper limit of τ since the actual ion density for C and Al is less, ~20%of total ions (obtained from the estimate of the plasma composition from another similar experiment[17]). Therefore, the opacity effect is negligible in the present conditions.

Close to the anode surface ($0 \le z \le 0.5$ mm) and for $r < 8$ mm, the line shapes are Stark dominated (due to the higher density), prohibiting the B-field determination with a reasonable error bar. In the radially outer region ($r = 8$ mm), n_e is relatively lower and an upper limit of the magnetic field can be determined from the analysis of the detailed shape of the Al III 5722 Å line. A blow up of the Al III 5722 Å line at $z = 0.25$ mm and $r = 8$ mm along with different fits, obtained by varying the Lorentzian component and assuming $B_\theta = 0$, 0.8 T, and 1.2 T, is shown in Fig. 6. As demonstrated in the figure, the fits do not change much up to $B_\theta = 1.2$ T; assuming $B_\theta > 1.2$ T, a reasonable fit cannot be obtained for any Lorentzian. Therefore, for this point, only an upper limit of the field ($B_\theta \le 1.2$ T) can be determined.

Figure 7 shows the values of B_θ obtained for the various radial positions. It is seen that the B_θ-values obtained from

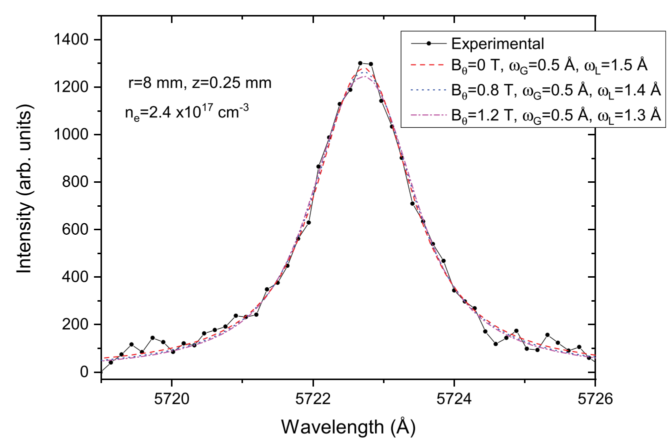

FIG. 6. Al III $4s - 4p\,^3S_{1/2} - ^3P_{1/2}$ 5722 Å line, along with different fits, recorded from the region of $0 \le z \le 0.5$ mm at $r = 8$ mm.

the C IV line are higher than those obtained from the Al III lines even though the spectrum of the two ions is collected by the same fiber focused at $z = 0.75$ mm. Indeed, it was shown in Sec. III that the intensity ratio of the C IV-to-Al III lines increases with the distance from the anode. Thus, the Zeeman effect of the C IV line tends to reflect the B-field farther from the anode than the Al III line. For simplicity, we assume here that the Al III line gives the B_θ value over half of the fiber field of view in the z-direction that is closer to the anode surface, namely, $z = 0.625 \pm 0.125$ mm, whereas the C IV line gives B_θ at $z = 0.875 \pm 0.125$ mm.

We now discuss the errors in the measurements. The errors indicated in the figure represents the uncertainties in determining the Zeeman splitting (for $r = 8$ mm and $z = 0.75$ mm) or in the fit of the line shapes. B_θ corresponding to the best fit (minimum of χ^2) of the line-shape is represented by the symbols in the figure. The lower and upper values of B_θ correspond to an increase of 20% in χ^2. For $r < 8$ mm, we find that a reasonable fit can be obtained even when $B_\theta = 0$ is assumed. This can be understood by the fact

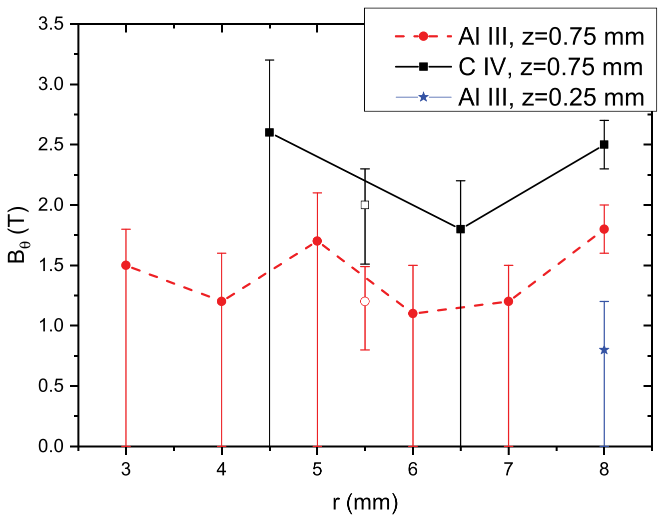

FIG. 7. Radial distribution of B_θ obtained from the fit of the line-shape of C IV $3s-3p\,{}^3S_{1/2}-{}^3P_{1/2}$ (black square) and Al III $4s-4p\,{}^3S_{1/2}-{}^3P_{1/2}$ (red circle) transitions. The data points at $r=4.5$ mm and $r=6.5$ mm for C IV are averages over the signals at $r=4$ and 5 mm and $r=6$ and 7 mm, respectively. Open symbols denote the average value of B_θ in the radial region at $4\le r\le 7$ mm and $0.5\le z\le 1$ mm.

that when no Zeeman-split pattern is observed, the broadening of the spectral line due to the Zeeman effect can be reasonably reproduced by Stark broadening. On the other hand, the absence of an observed splitting provides a clear upper limit on the assumed B_θ. We note that if we sum up the emissions from $r=4$ mm to $r=7$ mm after the "onion peeling" procedure, flat-top line shapes are obtained with significantly improved S/N ratios. The analysis of these line-shapes yields the average B_θ values in the region 4 mm $\le r\le$ 7 mm with much smaller uncertainty, as shown in Fig. 7.

V. SHIELDING OF THE MAGNETIC FIELD

The lower value of B_θ towards the anode surface, seen in Fig. 7, demonstrates the shielding of the magnetic field by the internal currents in the anode plasma. The low B_θ value obtained from the Al III line recorded from the region $z=0.25\pm0.25$ mm (i.e., fibres viewing the region closer to the anode surface) is consistent with the expected stronger shielding effect deeper in the anode plasma.

We now attempt to explain the shielding effect of B in the anode plasma by considering the measurements for $r=8$ mm since at this radial position, B_θ is determined with the highest accuracy. Here, at $z=0.875$ mm, the observed B is 2.5 T, giving a current of 100 kA within this radius (out of the total 120 kA measured by a B-dot probe at this time). The true total current within $r=8$ mm can be 100 kA, if no shielding effect occurs for the data point at $r=8$ mm and $z=0.875$ mm, or it can be between 100 and 120 kA, if shielding occurs to some extent. In either case, if the total current within $r=8$ mm is <120 kA, then part of the current in the diode flows to the anode surface outside the $r=8$ mm region (note that the cathode radius is 5 mm).

For simplicity, we assume here that the total current flows within $r=8$ mm, namely, the unshielded-B value at this radius and at the plasma edge in the z-direction is 3 T. Also, for simplicity, we assume that the anode-plasma thickness in the z-direction at $r=8$ mm is ~1 mm, and it is constant in time. Thus, the B_θ field at $r=8$ mm and $z=1$ mm rises in time to a value of 3 T (corresponding to the value of 120 kA at the time of the measurement), where the rise in time can be obtained from the measured current waveform. With these assumptions, we can consider the diffusion equation

$$\frac{\partial \mathbf{B}}{\partial t}=-\frac{c^2}{4\pi}\nabla\times(\eta\nabla\times\mathbf{B}), \tag{1}$$

where η is the plasma resistivity and c is the speed of light in free space. Here, we have neglected the convective and Hall terms, which is justified for our plasma conditions. Equation (1) can be written as

$$\frac{\partial \mathbf{B}}{\partial t}=-\frac{c^2}{4\pi}\left[-\eta\nabla^2\mathbf{B}+\nabla\eta\times(\nabla\times\mathbf{B})\right]. \tag{2}$$

For a uniform plasma resistivity, the second term in the right hand side (rhs) of Eq. (2) vanishes, and the equation for $\mathbf{B}=B_\theta\hat{\boldsymbol{\theta}}$ becomes

$$\frac{\partial B_\theta}{\partial t}=\frac{c^2\eta}{4\pi}\left[\frac{1}{r}\frac{\partial}{\partial r}\left(r\frac{\partial B_\theta}{\partial r}\right)+\frac{\partial^2 B_\theta}{\partial\xi^2}-\frac{B_\theta}{r^2}\right], \tag{3}$$

where $\xi=z\text{–}z_0$, the distance from the plasma boundary at $z=z_0$. Assuming realistic possibilities for current density $J(r)$ near $r=8$ mm, it can be shown that Eq. (3) can be approximated to within very few percent by

$$\frac{\partial B_\theta}{\partial t}=\frac{c^2\eta}{4\pi}\frac{\partial^2 B_\theta}{\partial\xi^2}, \tag{4}$$

and this is the one dimensional diffusion equation; the boundary conditions for B_θ for our experimental condition are

$$B_\theta(\xi,0)=0, \tag{5}$$
$$B_\theta(\xi=0,t)=B_0(t).$$

A simple solution of Eq. (4) can be made for an infinite plasma thickness (i.e., plasma thickness, $l\gg$ skin depth, δ). However, in the present case, $l\sim\delta$. Therefore, B_θ is not zero at the conductive anode surface, which affects the B_θ distribution in the plasma. Thus, in our solution, $\eta=\eta(z)$ is composed of the resistivity (η_1) of the plasma and a step change in the resistivity (η_2) of the conductive anode at the anode surface. η_1 is estimated from the electron temperature in the plasma, which is determined to be 5–6 eV from line intensity ratios that were measured in a similar experiment.[9,14] This analysis also yielded that $\bar{Z}$ in the plasma is 2.5 ± 0.5, giving a Spitzer resistivity of $4.8\pm1.4\times10^{-15}$ s. For the conductive anode, we use $\eta_2=10^{-17}$ s. Using $\eta=\eta(z)$ in Eq. (2), it becomes

$$\frac{\partial B_\theta}{\partial t}=\frac{c^2}{4\pi}\left[\eta\frac{\partial^2 B_\theta}{\partial\xi^2}+\frac{\partial\eta}{\partial\xi}\frac{\partial B_\theta}{\partial\xi}\right]. \tag{6}$$

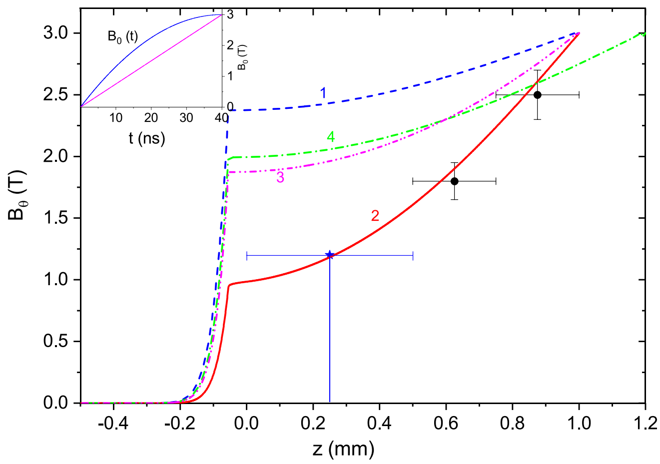

FIG. 8. Solution of the magnetic field diffusion in the plasma taking into account the effect of the metal-anode by considering a plasma resistivity η_1 constant over time and space and a resistivity $\eta_2 = 10^{-17}$ s for the metallic anode. $z = 0$ is the interface of the anode surface and the plasma. Symbols with the error-bars are the measured values, and "*" (blue-color) denotes the estimated upper limit of B_θ (see Sec. IV). Curves 1 and 2 represent the solutions for a plasma resistivity $\eta_1 = 4.8 \times 10^{-15}$ s (that corresponds to the Spitzer resistivity for $T_e = 5$ eV) and a $3\times$ lower resistivity that gives the best fit for the data, respectively. For these two curves, assumed is a parabolic waveform for B_0, i.e., $B_0(t) = -[B_0(t = t_{max})/t_{max}^2](t - t_{max})^2 + B_0(t = t_{max})$ and a constant plasma thickness $l = 1$ mm. In all solutions, the diffusion time t_{max} is assumed to be 40 ns, and $B_0(t_{max})$, the value of B_θ at the plasma edge at the time of measurement, is assumed to be 3 T. Curves 3 and 4 show the sensitivities of the solution to the shape of the waveform of B_0 and the value of l, respectively. The solution for a linear (instead of a parabolic) waveform of B_0, i.e., $B_0(t) = [B_0(t = t_{max})/t_{max}]t$, and for $l = 1$ mm is shown by curve 3, and the solution for $l = 1.2$ mm (instead of $l = 1$ mm) and for a parabolic waveform of $B_0(t)$ is shown by curve 4. Both parabolic and linear waveforms of B_0 are shown in the upper left corner of the figure.

Equation (6) is solved numerically with the boundary conditions described in Eq. (5) for various assumptions relevant to the experimental conditions, as shown in Fig. 8. $B_0(t)$ is taken to be either parabolic or linear in time since the diode-current waveform is between these two shapes. The value of the field at the plasma outermost point (i.e., at $\xi = 0$) is assumed to rise to 3 T; the experimental data indicate a value between 2.5 T and 3 T, as discussed above. The thickness of the plasma l is taken to be constant in time; solutions are given for 1 mm and 1.2 mm to indicate the sensitivity.

Curves 1 and 2 in Fig. 8 give the solutions for the same assumptions but for the Spitzer resistivity value and a value that is $3\times$ lower, respectively; the lower resistivity value seems to provide a better fit for the data. However, the solutions for different assumptions, still consistent with the data (curves 3 and 4), indicate that a plasma resistivity closer to the Spitzer value can also fit the data. Also, assuming a maximum $B_0(t)$ between 2.5 T and 3 T (rather than 3 T) tends to make the resistivity value that fits the data higher (namely, closer to the Spitzer value). Thus, as seen from these solutions, within the uncertainties due to the assumptions for the solution, and the uncertainty in the Spitzer-resistivity value mentioned above, a plasma resistivity that is close to the Spitzer value appears to be consistent with the magnetic field diffusion observed.

The distribution of the maximum (unshielded) B-field value cannot be determined for each radius from these data since the shielding may be occurring at different extents for the different positions viewed in the anode plasma. Knowledge of the total current within the central, 3-mm-radius, x-ray spot size could help assess the shielding extent. However, this quantity is not known well as outlined in Ref. 3. As an instructive note, if, for example, the current in the x-ray spot is 60 kA, then all the data points due to the Al III line demonstrate the shielding of B_θ in the plasma (since all these data points give magnetic fields lower than the expected from the current within the spot). If the current is 90 kA, then also the points due to the C IV line at $r = 4.5$ mm and $r = 6.5$ mm demonstrate the shielding of B_θ.

VI. CONCLUSIONS

Simultaneous measurements of the azimuthal magnetic field B_θ and the electron density n_e near the anode surface of a relativistic SMP diode are performed using detailed line shape calculations of the observed Al III $4s$–$4p$ and C IV $3s$–$3p$ doublet emissions. The measurement of B_θ as a function of r, and for different distances from the anode surface, yielded information on the shielding of the B-field by the anode plasma and on the plasma resistivity. The unknown extent of the field shielding at each radius does not allow for determining uniquely the radial distribution of the current-density over the anode surface.

ACKNOWLEDGMENTS

We are grateful to Tim Webb and Nichelle Bennett for numerous discussions regarding the physics of the SMP diode, as well as to the RITS crew, who provided the technical support required for conducting the experiments. Valuable discussions with Evgeny Stambulchik, Alexander Starobinets, and Christine Stollberg are highly appreciated.

Sandia National Laboratories is a multimission laboratory managed and operated by National Technology & Engineering Solutions of Sandia, LLC, a wholly owned subsidiary of Honeywell International Inc., for the U.S. Department of Energy's National Nuclear Security Administration under Contract No. DE-NA0003525. This paper describes objective technical results and analysis. Any subjective views or opinions that might be expressed in the paper do not necessarily represent the views of the U.S. Department of Energy or the U.S. Government.

[1]J. Maenchen, G. Cooperstein, J. O'Malley, and I. Smith, Proc. IEEE **92**, 1021 (2004).
[2]S. Swanekamp, G. Cooperstein, J. Schumer, D. Mosher, F. Young, P. F. Ottinger, and R. Commisso, IEEE Trans. Plasma Sci. **32**, 2004 (2004).
[3]K. D. Hahn, N. Bruner, M. D. Johnston, B. V. Oliver, T. J. Webb, D. R. Welch, S. R. Cordova, I. Crotch, R. E. Gignac, J. J. Leckbee, I. Molina, S. Portillo, J. R. Threadgold, and D. Ziska, IEEE Trans. Plasma Sci. **38**, 2652 (2010).
[4]P. Martin, J. Threadgold, and S. Vickers, IEEE Trans. Plasma Sci. **41**, 2510 (2013).
[5]B. V. Oliver, K. Hahn, M. D. Johnston, and S. Portillo, Acta Phys. Pol., A **115**, 1044 (2009).
[6]N. Bruner, D. R. Welch, K. D. Hahn, and B. V. Oliver, Phys. Rev. Spec. Top.-Accel. Beams **14**, 024401 (2011).
[7]Y. Maron, E. Sarid, E. Nahshoni, and O. Zahavi, Phys. Rev. A **39**, 5856 (1989).
[8]Y. Maron, E. Sarid, O. Zahavi, L. Perelmutter, and M. Sarfaty, Phys. Rev. A **39**, 5842 (1989).

[9]S. G. Patel, M. D. Johnston, T. J. Webb, N. L. Bennett, D. R. Welch, R. M. Gilgenbach, M. E. Cuneo, M. L. Kiefer, J. J. Leckbee, M. G. Mazarakis, D. J. Muron, T. J. Renk, S. C. Simpson, R. Doron, S. Biswas, D. Mikitchuk, and Y. Maron, Rev. Sci. Instrum. **89**, 10D123 (2018).
[10]R. P. Golingo and U. Shumlak, Rev. Sci. Instrum. **74**, 2332 (2003).
[11]E. Stambulchik, K. Tsigutkin, and Y. Maron, Phys. Rev. Lett. **98**, 225001 (2007).
[12]S. Tessarin, D. Mikitchuk, R. Doron, E. Stambulchik, E. Kroupp, Y. Maron, D. Hammer, V. Jacobs, J. Seely, B. Oliver, and A. Fisher, Phys. Plasma **18**, 093301 (2011).
[13]R. Doron, D. Mikitchuk, C. Stollberg, G. Rosenzweig, E. Stambulchik, E. Kroupp, Y. Maron, and D. A. Hammer, High Energy Density Phys. **10**, 56 (2014).
[14]M. D. Johnston, S. G. Patel, R. E. Falcon, K. Cartwright, M. L. Kiefer, M. E. Cuneo, and Y. Maron, "Measuring plasma formation, field strength, and current loss in pulsed power diodes," Sandia National Laboratories Report No. SAND2017-12565 (2017).
[15]E. Stambulchik and Y. Maron, J. Quant. Spectrosc. Radiat. Transfer **99**, 730 (2006).
[16]N. Konjević, A. Lesage, J. R. Fuhr, and W. L. Wiese, J. Phys. Chem. Ref. Data **31**, 819 (2002).
[17]R. Doron, S. Biswas, V. Bernshtam, E. Stambulchik, Y. Maron, M. D. Johnston, S. G. Patel, M. L. Kiefer, and M. E. Cuneo, "Determination of the plasma composition using blended Stark-Broadened emission lines in a self-magnetic pinch diode," (unpublished).